Supporting Information

Fedosov et al. 10.1073/pnas.1101210108

SI Results and Discussion

The structure factor $S(\mathbf{q})$ is often employed to characterize the structure of a suspension because it is directly accessible in scattering experiments. For a static system in three dimensions, $S(\mathbf{q})$ is defined as

$$S(\mathbf{q}) = \frac{1}{N}\sum_{j,k=1}^{N}\langle \exp[i\mathbf{q}\cdot(\mathbf{r}_j - \mathbf{r}_k)]\rangle = 1 + \rho_0 \int_{V_d} d^3r \exp(i\mathbf{q}\cdot\mathbf{r})[g(\mathbf{r}) - 1], \quad \textbf{[S1]}$$

where $\mathbf{q}$ is the scattering vector, $\mathbf{r}$ is a particle position, N is the total number of particles, $g(\mathbf{r}) - 1$ is the normalized pair correlation function, and ρ_0 is the particle density in the volume V_d.

The calculation of the structure factor in a particular direction (x, y, or z) shows no directional structure within the RBC suspension for various shear rates in agreement with the directional pair correlation function mentioned in the paper. The existence of local microstructure within the suspension can be checked through the isotropic structure factor $S(q)$, which can be calculated as

$$S(q) = \frac{1}{N}\sum_{j,k=1}^{N}\left\langle \frac{\sin(qr_{jk})}{qr_{jk}}\right\rangle, \quad \textbf{[S2]}$$

where $q = |\mathbf{q}|$ and $r_{jk} = |\mathbf{r}_j - \mathbf{r}_k|$. Analogously, $S(\mathbf{q})$ in Eq. **S1** can be integrated (averaged) over an orientational angle to obtain

$$S(q) = 1 + \frac{4\pi\rho_0}{q}\int_0^\infty [g(r) - 1]r\sin(qr)dr, \quad \textbf{[S3]}$$

where $g(r)$ is the radial distribution function. Fig. S1 presents the isotropic structure factor $S(q)$ for different shear rates and aggregation conditions calculated from simulation data using Eq. **S2**. We also verified that Eq. **S3** provides the same results using the radial distribution functions shown in Fig. 4*A* of the paper. For a comparison, if we look at the aggregating case with shear rate $\dot{\gamma} = 0.045\ \mathrm{s}^{-1}$ (dashed red curve), we notice that the last peak in $S(q)$ at $q = 2.7\ \mu\mathrm{m}^{-1}$ corresponds to the peak in $g(r)$ at $r = 2\pi/q = 2.33\ \mu\mathrm{m}$ (dashed red curve in Fig. 4*A* of the paper), which characterizes two-cell aggregates present separately or within larger aggregate structures. Analogously, we can relate other peaks of $S(q)$ curves to the corresponding peaks in $g(r)$ for various shear rates and aggregating conditions. The simulation data show that these two microstructure characterization approaches are equivalent, which is expected because $S(\mathbf{q})$ is simply the Fourier transform of $g(\mathbf{r}) - 1$.

Methods

We first briefly review the simulation method, the multiscale RBC (MS-RBC), and the low-dimensional RBC (LD-RBC) models, including the aggregation models. Then, we present details on the scaling from model units to physical units.

Dissipative Particle Dynamics. Dissipative particle dynamics (DPD) (1, 2) is a mesoscopic particle method, where each particle represents a molecular cluster rather than an individual atom, and can be thought of as a soft lump of fluid. The DPD system consists of N point particles, which interact through soft pairwise forces. The DPD system is kept at equilibrium temperature with a local thermostat. The time evolution of velocities and positions of particles is determined by the Newton's second law of motion. More details on the DPD method can be found elsewhere (1, 2).

The LD-RBC model employs colloidal particles in RBC construction. To simulate colloidal particles with rotational degrees of freedom by single DPD particles, we use a new formulation of DPD (3), in which the forces acting on a particle are explicitly divided into two separate components: central and shear (noncentral) components. This modification allows us to redistribute and hence balance the forces acting on a single particle to obtain the correct hydrodynamics. The resulting method was shown to yield the quantitatively correct hydrodynamic forces and torques on a single DPD particle (3), and thereby produce the correct hydrodynamics for colloidal particles (4). We refer the reader to refs. 3 and 4 for more details.

MS-RBC Model. The average equilibrium shape of an RBC is biconcave as measured experimentally (5) and is represented by

$$z = \pm D_0\sqrt{1 - \frac{4(x^2+y^2)}{D_0^2}}\left[a_0 + a_1\frac{x^2+y^2}{D_0^2} + a_2\frac{(x^2+y^2)^2}{D_0^4}\right], \quad \textbf{[S4]}$$

where $D_0 = 7.82\ \mu\mathrm{m}$ is the average diameter, $a_0 = 0.0518$, $a_1 = 2.0026$, and $a_2 = -4.491$. The surface area and volume of this RBC are equal to 135 $\mu\mathrm{m}^2$ and 94 $\mu\mathrm{m}^3$, respectively. In the simulations, the RBC membrane is represented by a set of points $\{\mathbf{x}_i\}$, $i \in 1\ldots N_v$ that are the vertices of a two-dimensional triangulated network on the RBC surface described by Eq. **S4** and shown in Fig. S2. The potential energy of the system is defined as follows:

$$V(\{\mathbf{x}_i\}) = V_{\text{in-plane}} + V_{\text{bending}} + V_{\text{area}} + V_{\text{volume}}, \quad \textbf{[S5]}$$

which includes the in-plane elastic energy $V_{\text{in-plane}}$ (springs), the bending energy V_{bending}, and the area and volume conservation constraints V_{area} and V_{volume}. The spring forces in the membrane model mimic the elastic energy of the spectrin network, and they are a combination of conservative elastic forces, which may be expressed in terms of the energy potential $V_{\text{in-plane}}$, and dissipative forces, which mimic viscous dissipation within the membrane. The bending energy represents the bending resistance of the lipid bilayer, whereas the area and volume energies enforce area incompressibility of the lipid bilayer and incompressibility of the inner cytosol, respectively. Detailed description of these potentials and membrane dissipative forces can be found in refs. 6–8.

Macroscopic elastic properties (shear, area compression, and Young's moduli) of modeled RBCs, as well as membrane viscosity, are analytically derived through a linear analysis of the regular hexagonal network (6, 7) resulting in a relationship between these macroscopic RBC properties and the network and model parameters. Thus, no parameter adjustment is performed.

RBCs are suspended in a solvent, which is represented by a collection of interacting DPD particles. To impose no-slip boundary conditions at the membrane, the DPD pairwise forces between fluid particles and membrane vertices are properly set; see refs. 7 and 8 for more details.

MS-RBC Aggregation Interactions. For blood, the attractive cell–cell interactions are crucial for simulation of aggregation into rouleaux. These forces are approximated phenomenologically with the Morse potential given by

$$U_M(r) = D_e[e^{2\beta(r_0-r)} - 2e^{\beta(r_0-r)}], \qquad \textbf{[S6]}$$

where r is the separation distance, r_0 is the zero force distance, D_e is the well depth of the potential, and β characterizes the interaction range. For the MS-RBC model, the Morse potential interactions are implemented between every two vertices of separate RBCs if they are within a defined potential cutoff radius r_d as shown in Fig. S3. The Morse interactions consist of a short-range repulsive force when $r < r_0$ and of a long-range attractive force for $r > r_0$. However, such repulsive interactions cannot prevent two RBCs from an overlap. To guarantee no overlap among RBCs, we employ a short-range Lennard–Jones potential and specular reflections of RBC vertices on membranes of other RBCs. The Lennard–Jones potential is defined as

$$U_{\mathrm{LJ}}(r) = 4\epsilon\left[\left(\frac{\sigma_{\mathrm{LJ}}}{r}\right)^{12} - \left(\frac{\sigma_{\mathrm{LJ}}}{r}\right)^{6}\right], \qquad \textbf{[S7]}$$

where ϵ and σ_{LJ} are energy and length characteristic parameters, respectively. These interactions are repulsive and vanish beyond $r > 2^{1/6}\sigma_{\mathrm{LJ}}$. In addition, specular reflections of RBC vertices on surfaces of other RBCs are necessary due to coarseness of the triangular network that represents the RBC membrane.

LD-RBC Model. The LD-RBC is modeled as a ring of 10 overlapping colloidal particles connected by springs (9). These colloids are single DPD particles whose repulsive point-force potentials define a hard surface which guarantees no overlap between cells. The radius of colloidal particles is equal to the radius of the ring of centers, and hence the configuration of the RBC is approximately a closed torus, as shown in Fig. S4. In addition to the springs interconnecting cell particles, the LD-RBC has bending resistance incorporated into the ring model between two consecutive springs. The model parameters are fitted through matching axial and transverse RBC deformations (9) with respect to the experimental data (10) for RBC stretching by optical tweezers. Because the thickness of the LD-RBC model is constant, the variations of the RBC volume and surface area were estimated under stretching and were found to vary by less than 8% in the range of all stretching forces (9). Therefore, the surface area and the volume constraints are approximately satisfied for the LD-RBC. The LD-RBC cell volume is approximately 158 μm^3, which is about 50% larger than MS-RBC volume. The LD-RBC has the same radius, but is thicker than an MS-RBC. The effect of coarse graining on stretching response was examined by varying the number of particles (N_c) in the ring. Fig. S5 shows the RBC shape evolution from equilibrium (0 pN force) to 100 pN stretching force for different N_c. Fig. S5 shows that increasing the number of ring particles results in both a smoother RBC surface (9) and improved agreement with the experimental stretching data (10). For $N_c = 10$, the fit to the data is excellent, and hence 10-particle rings were employed for all simulations. This representation is the accurate minimalistic model that we employed in our studies.

LD-RBC Aggregation Model. Here, we also employ the Morse potential given in Eq. **S6** to model the total intercellular attractive interactions between center of mass of different LD-RBCs. Thus, r is calculated based on the center of mass of RBCs—i.e., r is equal to the distance between the center of mass of two RBCs minus the thickness of RBC. We chose r_0 to be 200 nm because it is reported to be in nanometer scale (11–13).

We also calculate the normal vector of each RBC ($\vec{n}_c$), which is used to determine if the aggregation occurs between two RBCs according to the angles formed by the normal vectors of these RBCs with their center line. The RBC normal vector is defined as

$$\vec{n}_c = \frac{\sum \vec{v}_k \times \vec{v}_{k+1}}{N_c}, \qquad \vec{v}_k = \mathbf{x}_k - \mathbf{x}_c, \qquad \textbf{[S8]}$$

where $\mathbf{x}_k$ is the position of the kth particle in each RBC and $\mathbf{x}_c$ is the position of the center of mass. The center line $\vec{v}_{cij}$ of two RBCs (cell i and cell j) is defined as $\mathbf{x}_{ci} - \mathbf{x}_{cj}$. The angle formed by the normal vector of one cell with the center line is determined by their dot product $d_i = (\vec{n}_{ci} \cdot \vec{v}_{cij})$. The aggregation interactions between two LD-RBCs are in effect only if $d_i > d_c$ and $d_j > d_c$, where d_c is the critical value chosen to be $cos(\pi/4)$. Thus, the critical angle (θ_c) to turn on/off the aggregation interactions is $\pi/4$. This value is found to be suitable to induce rouleaux formation, but exclude the disordered aggregation. The proposed aggregation algorithm can be further illustrated by a sketch in Fig. S6, where the aggregation between two neighboring RBCs is decided to be on/off according to their relative orientation.

Scaling of Model and Physical Units. The dimensionless constants and variables in the DPD model must be scaled with physical units. The superscript M denotes that a quantity is in "model" units, while P identifies physical units (SI units). We define the length scale as follows:

$$r^M = \frac{D_0^P}{D_0^M}\ \mathrm{m}, \qquad \textbf{[S9]}$$

where r^M is the model unit of length, D_0 is the cell diameter, and m stands for meters. The energy per unit mass ($k_{\mathrm{B}}T$) and the force unit (N denotes Newton) scales are given by

$$(k_{\mathrm{B}}T)^M = \frac{Y^P}{Y^M}\left(\frac{D_0^P}{D_0^M}\right)^2 (k_{\mathrm{B}}T)^P, \qquad \mathrm{N}^M = \frac{Y^P}{Y^M}\frac{D_0^P}{D_0^M}\ \mathrm{N}^P, \qquad \textbf{[S10]}$$

where Y is the membrane Young's modulus. The time scale is defined as

$$\tau = \frac{D_0^P}{D_0^M}\frac{\eta^P}{\eta^M}\frac{Y^M}{Y^P}\ \mathrm{s}, \qquad \textbf{[S11]}$$

where η is a characteristic viscosity (e.g., solvent or membrane).

Simulation Setup and Parameters. Here, we present details of the simulation setup and parameters. The model units are chosen to be $r^M = 1$, $\tau = 1$, and $(k_{\mathrm{B}}T)^M = 1$.

MS-RBC: Viscosity predictions. RBC suspension was subjected to linear shear flow with periodic Lees–Edwards boundary conditions (14). The computational domain had the size of 45.0× $32.0 \times 27.222\ r^M$, where 168 RBCs and 117,599 solvent particles were placed. RBCs were represented by 500 DPD particles forming a triangulated network on the surface defined in Eq. **S4**. The RBC diameter and the membrane Young's modulus were $D_0 = 8.06\ r^M$ and $Y_0 = 415.5\ (k_{\mathrm{B}}T)^M/(r^M)^2$, respectively, corresponding to $D_0 = 7.82$ μm and $Y_0 = 18.9$ μN/m in physical units. The membrane shear modulus was $\mu_0 = 106\ (k_{\mathrm{B}}T)^M/(r^M)^2$.

We employed the stress-free model (6, 7), which eliminates local membrane artifacts (stresses) due to the membrane triangulation. Thus, each spring assumed its own equilibrium length l_0^i, $i = 1 \ldots N_s$, which was set to the edge lengths after the RBC shape triangulation. We calculated spring parameters individually for each spring using the given parameters μ_0 and l_0^i (7). The area and volume constraints coefficients were set to $k_a = 4{,}900$, $k_d = 100$, and $k_v = 5{,}000$ (the notations are the same as in ref. 7). The bending rigidity k_c was set to 3×10^{-19} J, which is equal to approximately 70 $k_{\mathrm{B}}T$ at physiological temperature $T = 37\,^{\circ}\mathrm{C}$.

The membrane viscosity was set to be $12\eta_0$, where η_0 is the suspending fluid viscosity.

Interactions between different RBCs included the short-range repulsive Lennard–Jones potential defined in Eq. **7**. The corresponding potential parameters were set to $\epsilon = 1.0\ (k_BT)^M$ and $\sigma_{LJ} = 0.3\ r^M$. These repulsive interactions result in a thin layer next to an RBC membrane that cannot be accessed by other cells. This layer can be interpreted as a slight increase of the RBC volume. Therefore, the RBC volume was assumed to be slightly larger than that of the triangulated network ($V_0 = 92.45\ (r^M)^3$) due to the repulsive RBC–RBC interactions. The effective RBC volume was estimated from an analysis of the distance between surfaces of several RBCs in equilibrium and was equal to $V' = 105\ (r^M)^3$. The cell volume fraction or hematocrit was calculated as follows:

$$H = \frac{N_c V'}{V_t}, \qquad [12]$$

where N_c is the number of RBCs in the volume V_t.

RBC aggregation interactions were mediated by the Morse potential (Eq. **S6**). The Morse potential parameters were set to $D_e = 0.3\ (k_BT)^M, r_0 = 0.3\ r^M, \beta = 1.5\ (r^M)^{-1}$, and $r_d = 1.1\ r^M$. The choice of r_0 was correlated with the Lennard–Jones characteristic length $\sigma_{LJ} = 0.3\ r^M$. Other aggregation parameters were calibrated for a single point of the viscosity-shear-rate curve, while all other simulations were performed for the same set of parameters.

RBCs were suspended in a solvent simulated by a collection of free DPD particles which correspond to small fluid volumes of blood plasma. Three fluids with different viscosities were employed in simulations: (*i*) $\eta_0 = 8.1$; (*ii*) $\eta_0 = 26.3$; and (*iii*) $\eta_0 = 126.0$, where η_0 is given in units $(k_BT)^M\tau/(r^M)^3$. Different viscosities allowed us to simulate different ranges of shear rates in physical units because they affect the timescale defined in *Scaling of model and physical units*. For example, a fixed shear rate in simulations in model units corresponds to distinct shear rates in physical units if different fluid viscosities are used. Table S1 presents the DPD interactions between different particle types [solvent (S) and RBC vertices (V)] (1, 2). The energy unit in simulations was set to $0.1\ (k_BT)^M$ which was calculated according to the energy scale defined in *Scaling of model and physical units*. The number density of the suspending fluid was $n = 3$. Note that the membrane viscosity also had to be changed with respect to η_0 and was always equal to $12\eta_0$. The dissipative force coefficient γ for the $S - V$ interactions defines RBC-solvent boundary conditions. In simulations, a single solvent for the blood plasma and cytosol was used. This simplification allowed us to substantially reduce the computational cost and to be able to calculate blood viscosity over five orders of magnitude in shear rates.

To cover a wide range of shear rates, several viscosities were required. Limitations of the DPD method do not allow us to simulate high shear rates, whereas at very low shear rates, simulation results obtained by statistical averaging contain relatively larger errors. The maximum shear rate ($\dot\gamma$) is limited by the local Reynolds number defined as

$$Re = \frac{n\dot\gamma D_0^2}{\eta_0}, \qquad [S13]$$

where n is the fluid's density. Table S2 shows the simulated flow regimes and the corresponding shear rate ranges in physical units. The *Re* number in all simulations remained below 0.5. The corresponding shear rates in physical units were calculated using the value of plasma viscosity $\eta_0 = 0.0012$ Pa at physiological temperature $T = 37$ °C.

MS-RBC: Maximum RBC aggregation force. The maximum aggregation force between two RBCs was computed in simulations with the aggregation parameters described above. The first (lower) RBC was adhered to a wall, which was simulated by holding stationary 100 vertices at the RBC bottom. The other (upper) RBC was placed on top of the adhered RBC and was allowed to aggregate in equilibrium simulation. Then, the force was applied to the upper RBC in order to separate them (see Movies S4 and S5).

Several cases of the separation of two RBCs were considered. In the first case (Movie S4), the upper RBC was pulled up in the normal direction, where the force was applied to 200 RBC vertices on the RBC top. This setup corresponds to a uniform separation, which was characterized by a nearly homogeneous and full separation of the two RBC surfaces in contact. The maximum force needed to break up the two aggregated RBCs in this case was approximately 7 pN. In the second case (Movie S5), the upper RBC was pulled up in the normal direction through 50 RBC vertices on the RBC top. Such disaggregation of two RBCs resembled peeling off the upper cell of the other RBC with the maximum force required for disaggregation to be approximately 3 pN. Finally, in the third setup, the upper RBC was pulled along the tangential direction with the force applied to 50–150 RBC vertices on the RBC side. Such separation of two RBCs can be described as sliding of the upper cell on the lower RBC and required the force of about 1.5–3 pN.

To compute the disaggregation force in shear flow (Movie S6), we used the same simulation setup. A fluid was confined between two parallel plates, while the lower RBC was attached to the lower plate, and the upper plate was moving with constant velocity. We found that the shear stress required for the disaggregation of RBCs is equal to approximately 0.02 Pa. The shear stress was defined as $\dot\gamma\eta_0$, where $\dot\gamma$ is the imposed shear rate.

LD-RBC: Viscosity predictions. The DPD interactions among different particle types [solvent (S) and cell (C) particles] are listed in Table s3; see also ref. 9. Random force coefficients σ_{ij} for different interactions were obtained according to $\sigma_{ij} = \sqrt{2k_BT\gamma_{ij}}$ with the energy unit $0.1\ (k_BT)^M$. The number densities of solvent particles was set to be $n_S = 3.0$. The intracell spring and bending parameters were set to $L_{max} = 1.3\ r^M$, $\lambda_p = 0.0005\ r^M$, and $k_b = 50\ (k_BT)^M$; see ref. 9 for details. The Morse potential parameters were chosen as $D_e = 500\ (k_BT)^M$, $\beta = 3.0\ (r^M)^{-1}$, and $r_0 = 0.1\ r^M$.

At the first glance, the Morse potential parameters used in the MS-RBC and LD-RBC models seem to be different, so here we provide a clarification. The RBC diameter was equal to $D_0 = 8.06\ r^M$ and $D_0 = 4\ r^M$ for the MS-RBC and LD-RBC models, respectively. Therefore, one length unit in RBC models corresponded to approximately 1 and 2 μm in physical units for MS-RBC and LD-RBC, respectively (see *Scaling of model and physical units*). Hence, we obtain that $\beta = 1.5\ (r^M)^{-1}$ in MS-RBC and $\beta = 3.0\ (r^M)^{-1}$ in LD-RBC correspond to the same value of $\beta = 1.5\ \mu m^{-1}$ in physical units. Analogously, $r_0 = 0.3\ r^M$ in MS-RBC and $r_0 = 0.1\ r^M$ in LD-RBC correspond to 0.3 and 0.2 μm, respectively; the value of r_0 does not have a strong effect on the Morse potential values. Finally, the remaining Morse potential parameter D_e seems to be very different for both models. However, in LD-RBC, $D_e = 500\ (k_BT)^M$ corresponds to the strength of aggregation interactions between two RBCs, because the aggregation force acts between two RBC centers of mass. In MS-RBC, $D_e = 0.3\ (k_BT)^M$ corresponds to local vertex–vertex interactions of two RBCs. Typically, 100–200 vertices of one RBC apply aggregation forces on the vertices of the other RBC, where each vertex of the former RBC interacts with 8–12 vertices of the latter RBC. Thus, the strength of aggregation interactions between two RBCs in MS-RBC can be estimated as $D_e \times 150 \times 10 = 450\ (k_BT)^M$, which is close to the corresponding value of the LD-RBC model.

1. PJ Hoogerbrugge, JMVA Koelman (1992) Simulating microscopic hydrodynamic phenomena with dissipative particle dynamics. *Europhy Lett* 19:155–160.
2. RD Groot, PB Warren (1997) Dissipative particle dynamics: Bridging the gap between atomistic and mesoscopic simulation. *J Chem Phys* 107:4423–4435.
3. W Pan, IV Pivkin, GE Karniadakis (2008) Single-particle hydrodynamics in dpd: A new formulation. *Europhys Lett* 84:10012.
4. W Pan, B Caswell, GE Karniadakis (2010) Rheology, microstructure and migration in Brownian colloidal suspensions. *Langmuir* 26:133–142.
5. EA Evans, R Skalak (1980) *Mechanics and Thermodynamics of Biomembranes* (CRC, Boca Raton, FL).
6. DA Fedosov, B Caswell, GE Karniadakis (2010) Systematic coarse-graining of spectrin-level red blood cell models. *Comput Methods Appl Mech Eng* 199:1937–1948.
7. DA Fedosov, B Caswell, GE Karniadakis (2010) A multiscale red blood cell model with accurate mechanics, rheology, and dynamics. *Biophys J* 98:2215–2225.
8. DA Fedosov (2010) *Multiscale modeling of blood flow and soft matter.* PhD thesis, Brown University, Providence, RI.
9. W Pan, B Caswell, GE Karniadakis (2010) A low-dimensional model for the red blood cell. *Soft Matter* 6:4366–4376.
10. S Suresh, et al. (2005) Connections between single-cell biomechanics and human disease states: Gastrointestinal cancer and malaria. *Acta Biomater* 1:15–30.
11. S Chien, K.-M Jan (1973) Ultrastructural basis of the mechanism of rouleaux formation. *Microvasc Res* 5:155–166.
12. B Neu, HJ Meiselman (2002) Depletion-mediated red blood cell aggregation in polymer solutions. *Biophys J* 83:2482–2490.
13. Y Liu, WK Liu (2006) Rheology of red blood cell aggregation by computer simulation. *J Comput Phys* 220:139–154.
14. AW Lees, SF Edwards (1972) The computer study of transport processes under extreme conditions. *J Phys C Solid State Phys* 5:1921–1928.

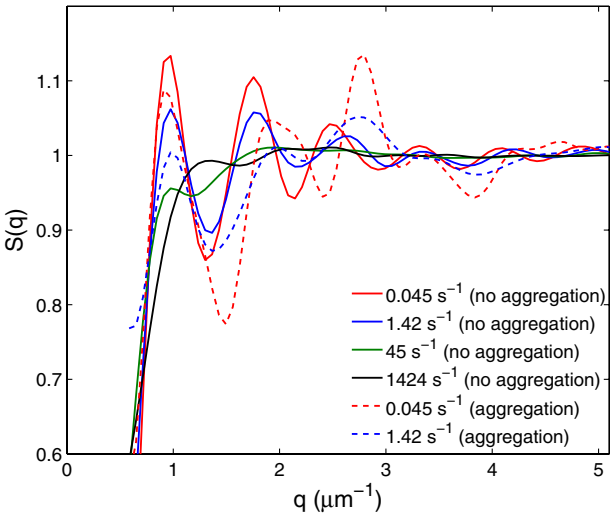

Fig. S1. Isotropic structure factor $S(q)$ for different shear rates with and without aggregation.

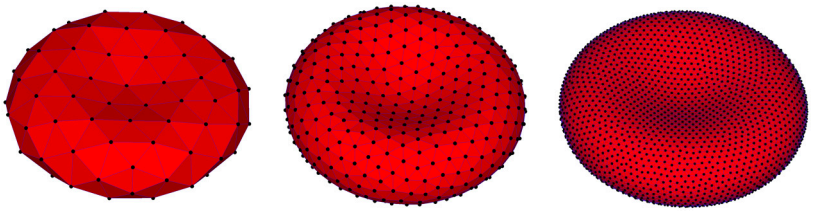

Fig. S2. MS-RBC membrane model with $N_v = 100$, 500, and 3,000 from left to right, respectively.

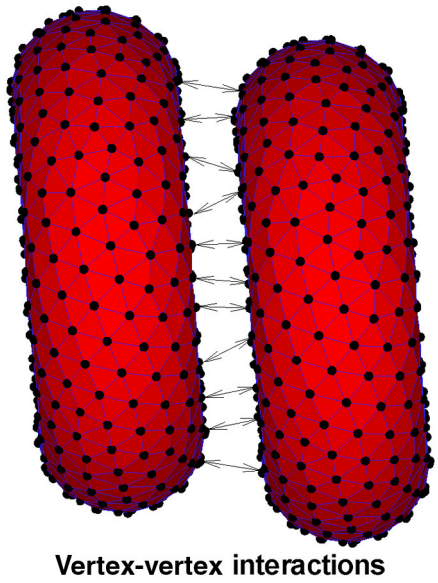

Fig. S3. MS-RBC: Aggregation interactions for the MS-RBC model.

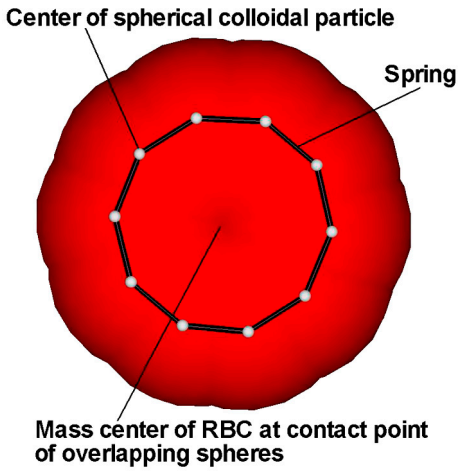

Fig. S4. LD-RBC: A sketch of the low-dimensional closed-torus-like RBC model.

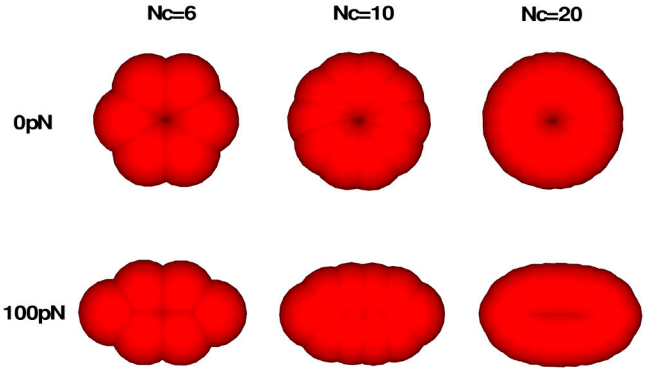

Fig. S5. LD-RBC shape evolution at different N_c (number of particles in LD-RBC model) and stretching forces.

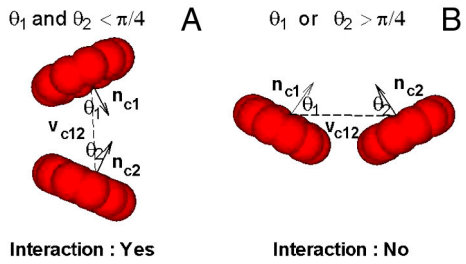

Fig. S6. Schematic of the aggregation algorithm. Here, the two neighboring RBCs (1 and 2) are to aggregate or not according to that the angles, θ_1 and θ_2, are smaller or greater than $\pi/4$.

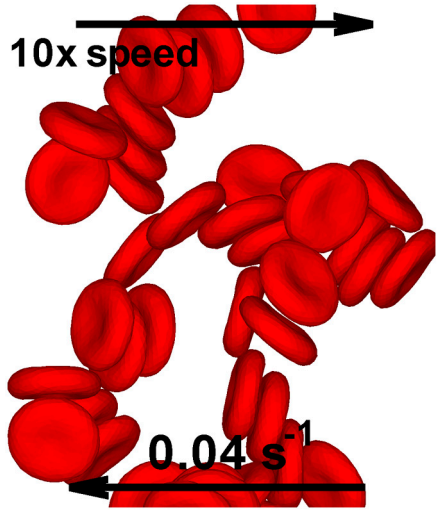

Movie S1. Simulation of MS-RBCs under shear flow at $H = 0.1$. Low shear rate of $\dot{\gamma} = 0.04$ s^{-1} results in a formation of relatively long rouleaux structures. Ten times the normal movie speed.

Movie S1 (MOV)

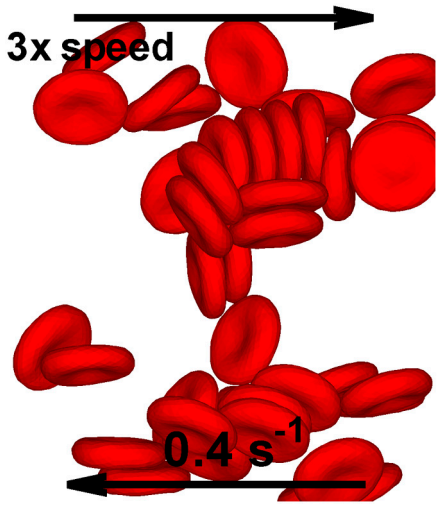

Movie S2. Simulation of MS-RBCs under shear flow at $H = 0.1$. Intermediate shear rate of $\dot{\gamma} = 0.4$ s^{-1} results in a formation of medium size (3–8 RBCs) rouleaux structures. Three times the normal movie speed.

Movie S2 (MOV)

Movie S3. Simulation of MS-RBCs under shear flow at $H = 0.1$. High shear rate of $\dot{\gamma} = 4.0\ s^{-1}$ results in essentially no rouleaux structures. Normal movie speed.

Movie S3 (MOV)

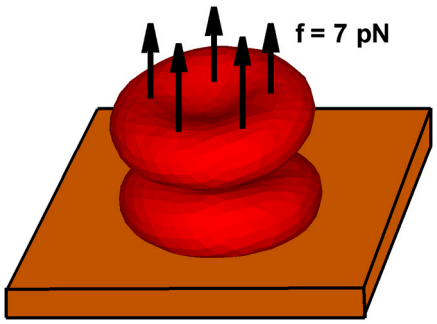

Movie S4. Simulation for computing the maximum force needed to break up two aggregated RBCs. The breakup pulling force in the normal direction is equal to about 7 pN with a uniform RBC-RBC separation.

Movie S4 (MOV)

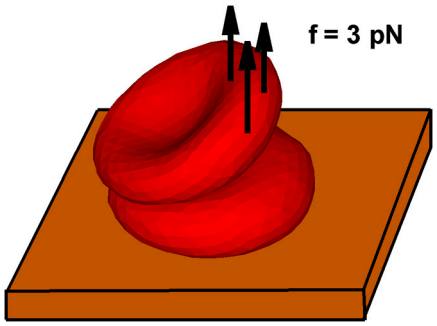

Movie S5. Simulation for computing the maximum force needed to break up two aggregated RBCs. The breakup pulling force in the normal direction is equal to about 3 pN with a peeling breakup.

Movie S5 (MOV)

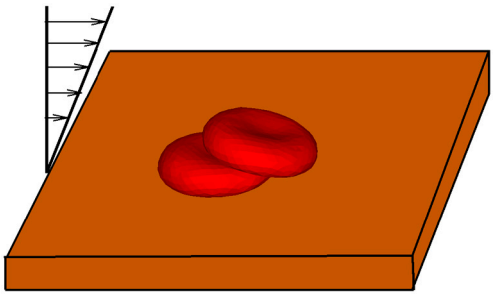

Movie S6. Simulation for computing the disaggregation force in shear flow yields the value of shear stress required to break up a rouleaux structure with the fluid shear stress value of about 0.02 Pa.

Movie S6 (MOV)

Table S1. MS-RBC: DPD simulation parameters

η_0	Interaction	a	γ	r_c	k (DPD envelope)
8.1	S–S	6.0	20.0	1.0	0.15
8.1	S–V	0.0	15.6	1.0	0.2
26.3	S–S	4.0	8.0	1.5	0.15
26.3	S–V	0.0	10.0	1.5	0.2
126.0	S–S	4.0	40.0	1.5	0.15
126.0	S–V	0.0	47.9	1.5	0.2

The parameters a and γ are the DPD conservative and dissipative force coefficients, r_c is the cutoff radius, and k is the exponent for the DPD envelope.

Table S2. MS-RBC: Simulated flow regimes and the corresponding shear rate ranges in physical units

η_0	$\dot{\gamma}$ in DPD	Re	$\dot{\gamma}$, s^{-1}
8.1	$5 \times 10^{-5} - 0.01$	0.0012–0.24	0.014–3.2
26.3	0.003–0.056	0.022–0.41	3.1–58
126.0	0.017–0.25	0.026–0.4	83–1,200

Table S3. LD-RBC: Parameters of DPD interactions in simulations

Interaction	Radial conservative force, linear	$\gamma^{\parallel} = \gamma^{\perp}$	r_c
S–S	$a = 2.5$	4.5	1.5
C–C (same cell)	$a = 500$	4.5	1.2
	radial conservative force, exponential		
C–C (different cell)	$a = 2{,}500$, $b = 20$, $r_c^e = 2.0$	4.5	2.0
S–C	$a = 2{,}500$, $b = 20$, $r_c^e = 1.0$	900	1.5

The parameters a, b, and r_c^e are the linear and exponential DPD conservative forces; $\gamma^{\parallel}$ and $\gamma^{\perp}$ are the dissipative force coefficients for central and shear force components, and r_c is the cutoff radius.